

# Thermoelectric Properties of Polycrystalline $\text{NiSi}_3\text{P}_4$

Andrew F. May,\* Michael A. McGuire, and Hsin Wang

*Materials Science and Technology Division, Oak Ridge National Laboratory, Oak Ridge, TN 37831*

The Hall and Seebeck coefficients, electrical resistivity and thermal conductivity of polycrystalline  $\text{NiSi}_3\text{P}_4$  were characterized from 2 to 775 K. Undoped  $\text{NiSi}_3\text{P}_4$  behaves like a narrow gap semiconductor, with activated electrical resistivity  $\rho$  below room temperature and a large Seebeck coefficient of  $\sim 400 \mu\text{V/K}$  at 300 K. Attempts to substitute boron for silicon resulted in the production of extrinsic holes, yielding moderately-doped semiconductor behavior with  $\rho$  increasing with increasing temperature above  $\sim 150$  K. Hall carrier densities are limited to approximately  $5 \times 10^{19} \text{cm}^{-3}$  at 200 K, which would suggest the solubility limit of boron is reached if boron is indeed incorporated into the lattice. These extrinsic samples have a Hall mobility of  $\sim 12 \text{cm}^2/\text{V/s}$  at 300 K, and a parabolic band equivalent effective mass of  $\sim 3.5$  times the free electron mass. At 700 K, the thermoelectric figure of merit  $zT$  reaches  $\sim 0.1$ . Further improvements in thermoelectric performance would require reaching higher carrier densities, as well as a mechanism to further reduce the lattice thermal conductivity, which is  $\sim 5 \text{W/m/K}$  at 700 K. Alloying in Ge results in a slight reduction of the thermal conductivity at low temperatures, with little influence observed at higher temperatures.

Copyright (2013) American Institute of Physics. This article may be downloaded for personal use only. Any other use requires prior permission of the author and the American Institute of Physics. The following article appeared in (J. Appl. Phys. 113, 103707 (2013)) and may be found at (this link)

## I. INTRODUCTION

Identifying thermoelectric materials composed of environmentally friendly and/or plentiful elements is one current thrust of the thermoelectric community. Recent successes in this area include several Zintl phases, such as  $\text{Ca}_3\text{AlSb}_3$  and  $\text{Ca}_5\text{Al}_2\text{Sb}_6$ .<sup>1,2</sup> Simple binaries such as  $\text{FeSb}_2$  and  $\text{FeSi}$  may be promising for low-temperature applications.<sup>3-5</sup> In addition to environmental concerns and abundance issues, low-density materials are also of interest for applications due to their potential for large specific powers, and the associated reduced mass requirements. For instance,  $\text{Mg}_2\text{Si}$  is an example of a material that possesses all of the above desired properties and good thermoelectric performance.<sup>6-8</sup> The higher manganese silicides ( $\text{MnSi}_{2-x}$ ,  $x \sim 0.25$ ) are another group of low-cost, abundant materials with promising thermoelectric performance.<sup>9,10</sup> It is this combination of abundant and low-density materials that brought us to examine another silicide,  $\text{NiSi}_3\text{P}_4$ , of which little is known beyond the crystallographic structure.

$\text{NiSi}_3\text{P}_4$  is isostructural with  $\text{Cu}_3\text{SbSe}_4$ ,<sup>11,12</sup> which has recently been shown to possess moderate thermoelectric performance. At the materials level, thermoelectric performance is quantified via the dimensionless figure of merit  $zT = \alpha^2 T / \rho \kappa$ , where  $\alpha$  is the Seebeck coefficient,  $\rho$  the electrical resistivity, and  $\kappa$  the thermal conductivity. In  $\text{Cu}_3\text{SbSe}_4$ ,  $zT$  reaches between 0.7 and 0.9 near  $\sim 650$  K, with the exact value depending on the particular alloying and doping employed.<sup>13-16</sup>

$\text{NiSi}_3\text{P}_4$  and  $\text{Cu}_3\text{SbSe}_4$  are isostructural with the mineral famatinite  $\text{Cu}_3\text{SbS}_4$ , which is a member of the stannite ( $\text{Cu}_2\text{FeSnS}_4$ ) group. These materials possess a tetragonal unit cell (space group  $I42m$ , No. 121) based

on the zinc-blende structure with all atoms being tetrahedrally coordinated (though the tetrahedral coordinations are slightly distorted with bond angles deviating from the ideal  $109.5^\circ$ ). In  $\text{Cu}_3\text{SbSe}_4$ , Cu and Sb are tetrahedrally coordinated by Se, whereas in  $\text{NiSi}_3\text{P}_4$ , Ni and Si are surrounded by P.

In this work, we characterize  $\text{NiSi}_3\text{P}_4$ , and find it to be a narrow gap semiconductor where holes naturally dominate conduction. This material is too resistive to yield large thermoelectric performance, and thus doping studies were undertaken. At first, we attempted to substitute Co for Ni, though this did not appear to produce extrinsic holes. Thus, in analogy with Si and SiGe alloys, we attempted to use boron as a hole dopant, and nominal compositions  $\text{NiSi}_{3-x}\text{B}_x\text{P}_4$  were found to produce extrinsic hole concentrations. If boron substitutes for silicon, it does so with a relatively limited solubility, as the maximum hole concentration observed in these samples is approximately  $5 \times 10^{19} \text{cm}^{-3}$  at 200 K. It is also possible the extrinsic hole concentration is associated with off-stoichiometry of the  $\text{NiSi}_3\text{P}_4$  phase induced by the nominal compositions employed. With some modest success at doping, it was clear that the lattice thermal conductivity severely limits the thermoelectric performance. Thus, we attempted to alloy in 20% Ge on the Si site, and this resulted in only a small decrease in  $\kappa$  (primarily at low temperatures). The net result is a rather low figure of merit  $zT \sim 0.1$  at 700 K. Further improvements in performance may be achieved with higher doping levels, as the material has a relatively high band mass, though a reduction in the lattice thermal conductivity is also necessary. Therefore, this material is unlikely to be pursued in further detail unless theoretical calculations provide insights into doping or suggest anomalous performance for other regions of the electronic structure.

## II. METHODS

Polycrystalline samples were prepared by first arc-melting high-purity Ni, Si, B, and Ge as appropriate for the nominal compositions listed in Table I. The resulting ingot was hand ground to a fine powder, and combined with red phosphorus in a silica ampoule that was subsequently sealed under vacuum. The ampoule was heated to 450 °C, held at this temperature for 10 h, then heated to 900 °C and held for 100 h to allow phosphorus to react through the vapor phase. After cooling, the ampoule was shaken vigorously and heated to 900 °C for another ~50-100 h to ensure full reaction of the phosphorus. During the first heating, a rate of 25 °C/h was employed, and 50 °C/h was used for the second heat treatment. Indications of decomposition and significant volatilization of phosphorus were observed when sintering of a cold-pressed pellet at 1000 °C was attempted, and thus ~900 °C was used as a high temperature limit.

After heating, the powders were hand ground and consolidated with a hot press. Hot pressing was performed in a graphite die within a graphite furnace, using pressures near 10,000 psi and a maximum temperature near 900 °C ± 50 °C. After exposure to the maximum force/temperature for ~1 h, the force was removed for a one hour stress-free anneal, followed by cooling to 675 °C over one hour, at which temperature the furnace was turned off to cool more rapidly. This procedure resulted in samples with densities greater than 92% of the crystallographic density. The samples are relatively stable in air, with only a very slight tarnish appearing after several months. Grinding was generally done in a helium glove box, though grinding in air prior to hot pressing did not appear to affect the transport properties provided the reaction was complete. The acrid smell of phosphorus was experienced upon cutting or grinding the final specimens.

The polycrystalline samples were found, by powder x-ray diffraction, to contain mainly the desired NiSi<sub>3</sub>P<sub>4</sub> phase. The undoped NiSi<sub>3</sub>P<sub>4</sub> sample contained a small amount (<2 wt.%) of Ni<sub>2</sub>Si. Rietveld refinement of the room temperature powder diffraction data using the published structural model<sup>11</sup> yielded lattice parameters of  $a=5.155(1)\text{\AA}$  and  $c=10.345(1)\text{\AA}$ . Boron substitution resulted in a negligible change in lattice parameters. With increasing nominal concentrations of boron, the impurity phase(s) changed from Ni<sub>2</sub>Si to BP and NiSi, with up to 3% and 6.4%, respectively, observed in sample 4,B in Table I. As discussed below, transport measurements suggest that the boron solubility limit was reached by the nominal composition of NiSi<sub>2.98</sub>B<sub>0.02</sub>P<sub>4</sub>. It is also possible that the phase width of NiSi<sub>3</sub>P<sub>4</sub> is reached at this nominal composition and boron does not incorporate into the lattice. In the sample with nominal composition NiSi<sub>2</sub>Ge<sub>0.6</sub>B<sub>0.4</sub>P<sub>4</sub>, the diffraction revealed about 87% purity of the main phase, with BP (7 wt.%) and Ge (6 wt.%) as the primary secondary phases. The lattice parameters indicate some Ge incorporated into the lattice, though, with refinement yielding  $a=5.169(1)\text{\AA}$  and

TABLE I. Nominal compositions and lattice parameters of the NiSi<sub>3</sub>P<sub>4</sub> and doped-NiSi<sub>3</sub>P<sub>4</sub> samples presented in this study.

| sample ID | nominal composition  | $a$<br>Å | $c$<br>Å  |
|-----------|--|----------|-----------|
| 1         | NiSi <sub>3</sub> P <sub>4</sub>                                     | 5.155(1) | 10.345(1) |
| 2, B      | NiSi <sub>2.98</sub> B <sub>0.02</sub> P <sub>4</sub>                | 5.155(1) | 10.345(1) |
| 3, B      | NiSi <sub>2.90</sub> B <sub>0.10</sub> P <sub>4</sub>                | 5.157(1) | 10.347(1) |
| 4, B      | NiSi <sub>2.80</sub> B <sub>0.20</sub> P <sub>4</sub>                | 5.154(1) | 10.342(1) |
| 5, B & Ge | NiSi <sub>2</sub> Ge <sub>0.6</sub> B <sub>0.40</sub> P <sub>4</sub> | 5.169(1) | 10.367(1) |

$c=10.367(1)\text{\AA}$ .

Transport data suggested very high hole concentrations are necessary to achieve large thermoelectric performance, and thus we attempted to synthesize samples with large concentrations of boron. The secondary phases seem to have little influence on the transport properties, as similar results were obtained on the different samples. To allow for an appreciation of the variations in properties across batches, we report data on several boron containing samples that possess similar transport properties and thus likely possess similar amounts of boron in the primary phase.

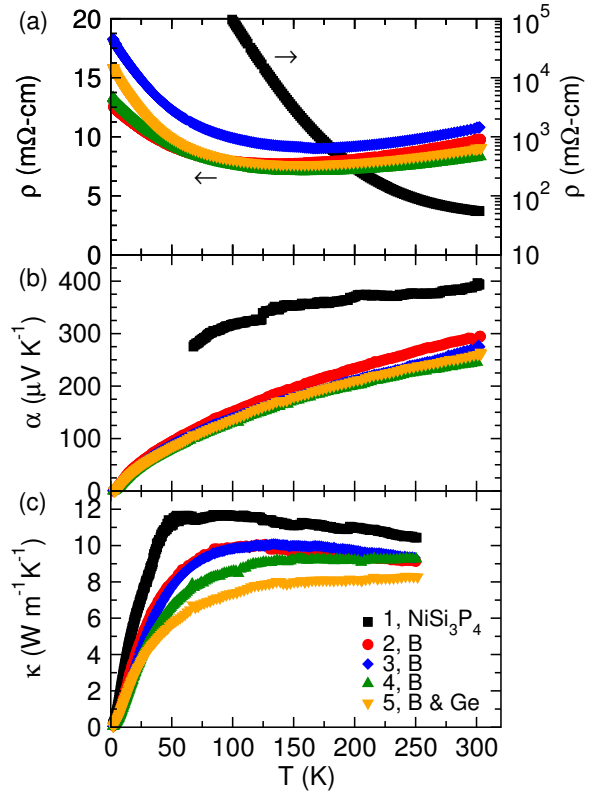


FIG. 1. (color online) (a) Electrical resistivity, (b) Seebeck coefficient, and (c) thermal conductivity of polycrystalline NiSi<sub>3</sub>P<sub>4</sub>, as well as B- and Ge-doped compositions as listed in Table I.

Seebeck coefficient  $\alpha$ , electrical resistivity  $\rho$ , and Hall coefficient  $R_H$  measurements were utilized to investigate the electrical properties; the Hall carrier density

is  $n_H=1/R_{He}$ . Below 300 K, these measurements were performed in a Quantum Design Physical Property Measurement System (PPMS). The thermoelectric measurements, including the thermal conductivity  $\kappa$ , were performed using the PPMS Thermal Transport Option (TTO), and the Hall effect was measured using the resistivity option on the PPMS. For TTO measurements, gold-plated copper leads were attached to the sample using silver epoxy (H20E Epo-Tek), and silver paste (DuPont 4929N) was utilized to obtain low resistance contacts for Hall effect measurements performed using 0.025 mm Pt wires. Hall coefficients were obtained from a fit of the Hall resistance versus magnetic field, with maximum fields of  $\pm 6$  Tesla employed.

High temperature thermoelectric performance was assessed using an ULVAC ZEM-3 M8 to measure  $\alpha$  and  $\rho$ . The thermal conductivity  $\kappa$  (above room temperature) was calculated via  $\kappa = D_T \times C_P \times d$  where  $d$  is the density. The specific heat capacity  $C_p$  was approximated using the Dulong Petit limit of  $C_v = 3R$ , calculated according to nominal composition. The differences between  $C_v$  and  $C_P$  are assumed to be negligible at the temperatures of interest, and this estimation likely results in a slight overestimation of  $zT$  at the highest temperatures. The thermal diffusivity  $D_T$  was obtained on  $\sim 10$  mm diameter discs between 1.5 and 2 mm thick, in an Anter FL-5000 with a graphite furnace; data analysis followed ASTM 1461 for flash diffusivity. No sign of oxidation occurred during the high temperature measurements, and data collected on cooling were consistent with those collected on heating.

### III. RESULTS AND DISCUSSION

NiSi<sub>3</sub>P<sub>4</sub> was found to behave similar to a narrow gap semiconductor with a low concentration of charge carriers. As shown in Figure 1, activated electrical conduction is observed for NiSi<sub>3</sub>P<sub>4</sub> below room temperature. Between 150 and 250 K, a simple activation energy was obtained from fitting to  $\rho = \rho_0 \text{Exp}[E_a/kT]$ , resulting in  $E_a = 0.11$  eV, which is equivalent to a fundamental band gap of 0.22 eV. However, the fit to this simple activated behavior becomes poor when wider temperature ranges are considered.

Consistent with the semiconducting-like behavior, a large Seebeck coefficient is observed in NiSi<sub>3</sub>P<sub>4</sub>, as shown in Figure 1b. Also consistent with this behavior, the Hall carrier density  $n_H$  increases with increasing temperature for NiSi<sub>3</sub>P<sub>4</sub>, as shown in Figure 2a. We emphasize that this is a single band  $n_H$ , and may not reflect the true carrier density if electrons are also contributing to electrical transport.

In order to probe the potential for thermoelectric performance, we attempted to hole-dope NiSi<sub>3</sub>P<sub>4</sub>. We first tried the substitution of Co for Ni, but this sample had a higher resistivity than undoped NiSi<sub>3</sub>P<sub>4</sub> at 300 K, and also displayed activated conduction below room temper-

ature. We then found that boron successfully increased the hole concentration in samples with nominal compositions of NiSi<sub>3-x</sub>B<sub>x</sub>P<sub>4</sub>. However, synthesis with  $x=0.02, 0.10, 0.20, 0.40$  all yielded similar transport properties, as observed in Figure 1. One explanation for this trend is that the solubility limit of boron has been reached.

Hole-doped samples of NiSi<sub>3-x</sub>B<sub>x</sub>P<sub>4</sub> behave metallic above  $\sim 150$  K with  $\rho$  increasing with increasing  $T$ . Similarly, the Seebeck coefficients of these samples increase with increasing  $T$ , consistent with extrinsically doped samples. The Seebeck coefficients remain rather large in these doped samples, with  $\alpha \sim 250 \mu\text{V/K}$  obtained at 300 K.

The Hall carrier concentration and mobility  $\mu_H$  of boron- and boron/germanium-doped NiSi<sub>3</sub>P<sub>4</sub> are shown in Figure 2. As observed, the values of  $n_H$  are relatively temperature independent, and fairly similar for the different nominal boron concentrations. This is consistent with similar  $\rho$  and  $\alpha$  in the various samples. This result suggests that, if boron substitutes for silicon, the solubility limit of boron has been reached. If lattice-incorporated boron atoms are fully ionized and contribute one hole to the system, then a solubility limit of  $\sim 0.2\%$  B per silicon is obtained from the Hall carrier concentration of approximately  $5 \times 10^{19}$  holes/cm<sup>3</sup> at 200 K. This seems reasonable considering the solubility limits of boron in silicon, which are  $\sim 2 \times 10^{19}$  B/cm<sup>3</sup> at 700°C and  $\sim 1 \times 10^{20}$  B/cm<sup>3</sup> at 900°C.<sup>17</sup> The small increase of  $n_H$  above  $\sim 200$  K may be the result of some carriers being activated from other impurities or across the band gap.

The hole mobility of boron-doped NiSi<sub>3</sub>P<sub>4</sub> is found to be approximately 12 cm<sup>2</sup>/V/s at 300 K. The mobility increases with decreasing temperature, consistent with a carrier mean free path limited by phonon scattering. However, this behavior only occurs down to  $\sim 125$  K, where the mobility reaches a maximum of approximately 18 cm<sup>2</sup>/V/s. While  $\mu_H$  decreases upon cooling below 125 K,  $n_H$  remains relatively constant, which may suggest that additional carrier scattering mechanisms are important at low  $T$ . Ionized impurity scattering generally leads to a mobility that increases as  $T^{3/2}$ , though the low- $T$  rise in  $\mu_H$  occurs more slowly than  $T^{3/2}$  in boron-doped NiSi<sub>3</sub>P<sub>4</sub>. It is also possible that Anderson localization occurs due to disorder in the lattice, causing a mobility gap that leads to an increase in  $\rho$  at low  $T$ . Also, we note that the high-temperature decay occurs more slowly than the  $T^{-3/2}$  behavior expected for a lightly doped semiconductor (or even the  $T^{-1}$  behavior expected for a degenerate semiconductor). Therefore, it is possible impurity band conduction is important in these materials or grain boundary scattering influences transport.

The hole mobility of boron-doped NiSi<sub>3</sub>P<sub>4</sub> is less than that of isostructural Cu<sub>3</sub>SbSe<sub>4</sub>. The mobility of undoped Cu<sub>3</sub>SbSe<sub>4</sub> is  $\sim 41$  cm<sup>2</sup>/V/s at 300 K, with a hole concentration of  $7.5 \times 10^{18}$  cm<sup>-3</sup>.<sup>13</sup> The mobility of undoped NiSi<sub>3</sub>P<sub>4</sub> is not shown in Figure 2 because the single band

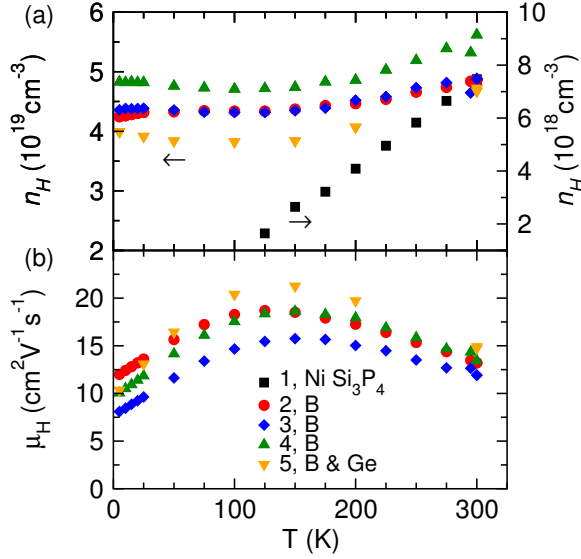


FIG. 2. (color online) (a) Hall carrier concentration and (b) Hall mobility of polycrystalline  $\text{NiSi}_3\text{P}_4$ , as well as B- and Ge-doped compositions as listed in Table I.

model likely fails for the undoped composition. At a more comparable hole concentration of  $6.3 \times 10^{19} \text{cm}^{-3}$  in  $\text{Cu}_3\text{Sb}_{0.975}\text{Sn}_{0.025}\text{Se}_4$  the mobility is approximately  $35 \text{cm}^2/\text{V/s}$ , and it is  $31 \text{cm}^2/\text{V/s}$  in  $\text{Cu}_3\text{Sb}_{0.95}\text{Sn}_{0.05}\text{Se}_4$  at 300 K.<sup>13</sup> Given that the carrier mobility in doped  $\text{NiSi}_3\text{P}_4$  is dominated by phonon scattering at room temperature, it seems unlikely that the boron dopant is leading to this large difference in carrier mobility. Therefore, the hole mobility in  $\text{NiSi}_3\text{P}_4$  appears to be inherently lower than in the copper-based analogues.

To better understand the differences between transport in  $\text{NiSi}_3\text{P}_4$  and  $\text{Cu}_3\text{SbSe}_4$ , we consider a parabolic band analysis of the Hall and Seebeck coefficients (Equations 1–4). Analysis of the Hall and Seebeck coefficient data allows the carrier mass  $m^*$  to be obtained. When phonon scattering limits the relaxation time of charge carriers, the mobility is expected to scale as  $\mu \propto m^{*-5/2}$ . Therefore, even small changes in the band mass can have significant influence on carrier transport.

Within a single parabolic band model, the Seebeck coefficient is a function of the reduced electrochemical potential  $\eta$  and scattering parameter  $\lambda$ :

$$\alpha = \frac{k}{e} \left( \frac{(2 + \lambda)F_{\lambda+1}(\eta)}{(1 + \lambda)F_{\lambda}(\eta)} - \eta \right). \quad (1)$$

The scattering parameter  $\lambda$  is used to incorporate the energy dependence of the carrier relaxation time,  $\tau = \tau_0 \epsilon^{\lambda-0.5}$ . The value of  $\lambda$  influences  $\alpha$ , but  $\tau_0$  does not. In this analysis, we assume acoustic phonon scattering limits  $\tau$ , corresponding to  $\lambda=0$ .

The Hall carrier density,  $n_H = 1/R_H e$  where  $R_H$  is the Hall coefficient, is given by

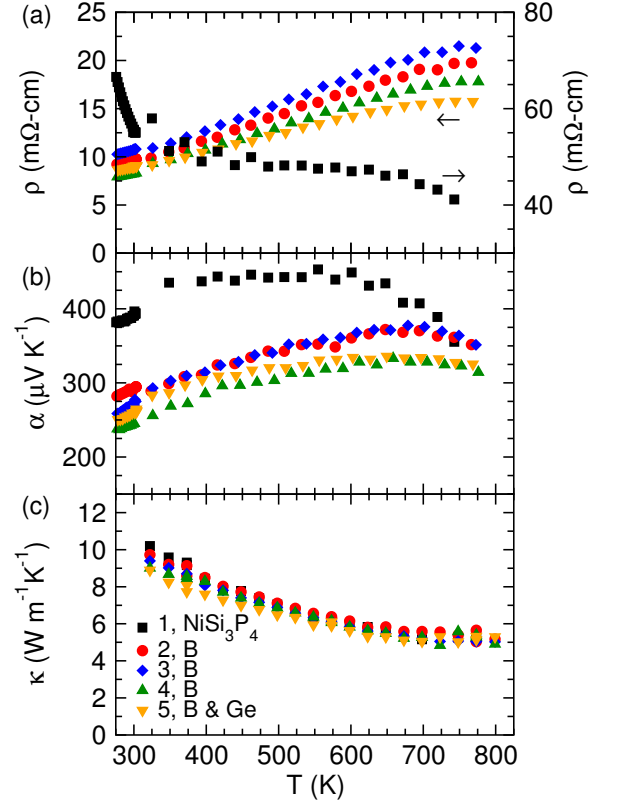


FIG. 3. (color online) High temperature (a) electrical resistivity, (b) Seebeck coefficient, and (c) thermal conductivity of polycrystalline  $\text{NiSi}_3\text{P}_4$ , as well as B- and Ge-doped compositions as listed in Table I.

$$n_H = 4\pi \left( \frac{2m^*kT}{h^2} \right)^{3/2} \frac{F_{1/2}(\eta)}{r_H}. \quad (2)$$

Analysis of  $n_H$  allows the effective mass  $m^*$  to be determined for a given  $\eta$  obtained from analysis of the Seebeck coefficient. Carrier scattering influences  $n_H$  through the Hall factor  $r_H$ , which is a function of  $\eta$  and  $\lambda$  similar to the Seebeck coefficient:

$$r_H = \frac{3}{2} F_{1/2}(\eta) \frac{(1/2 + 2\lambda)F_{2\lambda-1/2}(\eta)}{(1 + \lambda)^2 F_{\lambda}^2(\eta)}. \quad (3)$$

For simplification purposes, these expressions utilize the Fermi integrals  $F_j(\eta)$  defined by

$$F_j(\eta) = \int_0^\infty \frac{\xi^j d\xi}{1 + \text{Exp}[\xi - \eta]}. \quad (4)$$

Employing the above equations, we find that the effective mass is approximately  $3.5 \pm 0.5 m_e$  in boron-doped  $\text{NiSi}_3\text{P}_4$  at room temperature;  $m_e$  is the free electron

mass. At 200 K, where  $n_H$  is still relatively independent of temperature, this process yields  $2.9\text{--}3.7m_e$  for the various samples of boron-doped  $\text{NiSi}_3\text{P}_4$ . From literature values for  $n_H$  and  $\alpha$  in  $\text{Cu}_3\text{SbSe}_4$  (corresponding to the  $\mu$  values noted above),<sup>13</sup> we obtain  $0.45m_e < m^* < 1.3m_e$  depending on the particular sample. Therefore, it is clear that the band mass is much larger in  $\text{NiSi}_3\text{P}_4$  than in  $\text{Cu}_3\text{SbSe}_4$ , and this likely contributes to the lower mobility. This large band mass results in a relatively large Seebeck coefficient in  $\text{NiSi}_3\text{P}_4$ , but the impact on carrier mobility is detrimental to the thermoelectric performance of  $\text{NiSi}_3\text{P}_4$ .

The thermal conductivity of  $\text{NiSi}_3\text{P}_4$  is approximately  $10\text{ W/m/K}$  at 300 K. Boron doping reduces the low-temperature value of  $\kappa$  slightly. In an attempt to further reduce  $\kappa$ , we substituted Ge for Si, in addition to the boron doping. This results in some additional suppression of  $\kappa$  at low- $T$ , though little change is observed at higher temperatures. Interestingly,  $\kappa$  does not display much temperature dependence below room temperature, even in undoped  $\text{NiSi}_3\text{P}_4$ . This suggests there may be some disorder in the system, or perhaps grain boundaries or secondary phases are reducing  $\kappa$  at low- $T$ . We note that due to the large values of  $\rho$ , the lattice thermal conductivity  $\kappa_L$  dominates  $\kappa$  for all samples below  $\sim 600\text{ K}$ .

The high temperature transport properties are plotted in Figure 3. Interestingly, the decrease in  $\rho$  with increasing  $T$  for undoped  $\text{NiSi}_3\text{P}_4$  turns into a nearly temperature independent  $\rho$  above  $\sim 400\text{ K}$ , and the corresponding Seebeck coefficient is large and relatively temperature independent. The boron-doped samples display typical doped semiconductor behavior at high temperatures, with the resistivity and Seebeck coefficients increasing with increasing temperature until the effects of minority carrier activation are observed near 650 K. The thermal conductivity decreases with increasing  $T$  in all samples, consistent with the dominant role of phonon-phonon scattering in these crystalline materials. As noted above, the substitution of 20% Ge (nominal composition) did not result in a significant reduction in  $\kappa$  above 300 K. For comparison, the thermal conductivity of  $\text{Cu}_3\text{SbS}_4$  reaches approximately  $1.5\text{ W/m/K}$  at 600 K.<sup>13</sup>

The maximum in  $\alpha(T)$ , which is relatively unpronounced in these materials, can be utilized to estimate the thermal band gap by  $E_g = 2\alpha_{\max}T_{\max}$ .<sup>18</sup> This analysis suggests that the band gap is between 0.43 and 0.50 eV, which is about two times larger than that obtained from the analysis of  $\rho(T)$  at lower temperatures. It is possible that one of these estimates of  $E_g$  is influenced by the activation of carriers from an impurity band. Without high temperature Hall effect data the source for this discrepancy is difficult to isolate.

The thermoelectric power factor,  $\alpha^2 T/\rho$  is plotted in Figure 4 along with the figure of merit  $zT$ . Relatively low thermoelectric performance is observed in these materials. This is due in part to the relatively high thermal conductivity for the corresponding mobility val-

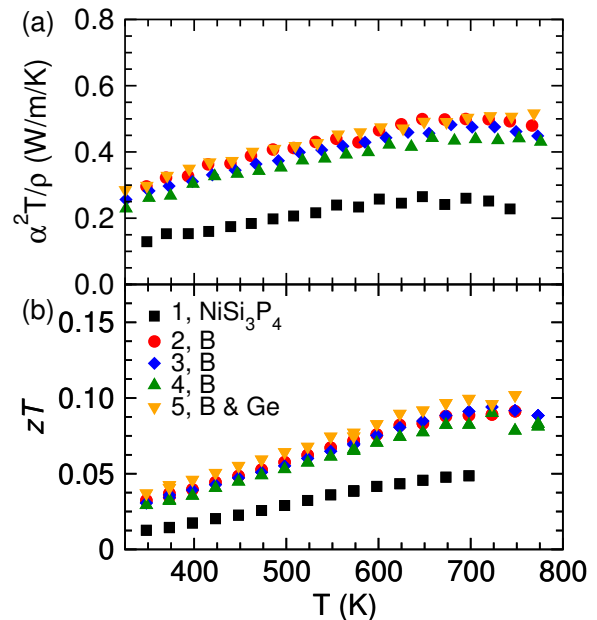


FIG. 4. (color online) (a) The thermoelectric power factor times temperature and (b) dimensionless figure of merit for polycrystalline  $\text{NiSi}_3\text{P}_4$ , as well as B- and Ge-doped compositions as listed in Table I.

ues. Boron-doping greatly improves both the power factor and  $zT$ , and additional improvements would likely come with higher doping levels. This is particularly the case for  $p$ -type  $\text{NiSi}_3\text{P}_4$ , because it is a large band mass material and the optimum carrier density increases with increasing band mass and increasing lattice thermal conductivity.<sup>19,20</sup> As noted, however, boron substitution only permits modest carrier densities to be reached, and using a transition metal dopant was not successful in increasing the hole concentration. It is possible that altering the Si/P ratio would permit higher doping levels to be achieved, and may also allow  $n$ -type behavior to be probed. However, it seems unlikely that this material will achieve the  $zT$  values observed in isostructural copper compounds, which have higher mobility due to lower band masses, as well as lower lattice thermal conductivities.

## A. Summary

Polycrystalline  $\text{NiSi}_3\text{P}_4$  was found to be a narrow gap semiconductor, with an activation energy for the electrical resistivity on the order of 100 meV below room temperature. Boron-doping is successful in producing extrinsic holes, though the corresponding hole concentration is limited to approximately  $5 \times 10^{19}\text{ cm}^{-3}$ , suggesting a possible solubility limit of boron in  $\text{NiSi}_3\text{P}_4$ . The transport properties of the boron-doped samples behave as expected for moderately doped semiconductors, and parabolic band analysis suggests a fairly high band mass

of  $\sim 3m_e$ . The thermoelectric figure of merit only reaches  $\sim 0.1$  at 700 K, due in large part to a lower than desired hole mobility and carrier concentration, and a moderately large thermal conductivity. Further improvements in thermoelectric performance may be possible with a different doping scheme or through additional phonon scattering, but are unlikely to yield large thermoelectric efficiencies.

#### IV. ACKNOWLEDGEMENTS

This research was supported by the U. S. Department of Energy, Office of Basic Energy Sciences, Materials Sciences and Engineering Division (A.F.M., M.A.M), and the US Department of Energy, EERE, Vehicle Technologies, Propulsion Materials Program (H.W.).

---

\* mayaf@ornl.gov

- <sup>1</sup> A. Zevalkink, E. S. Toberer, W. G. Zeier, E. Flage-Larsen, and G. J. Snyder, *Energy Environ. Sci.* **4**, 510 (2011).
- <sup>2</sup> E. S. Toberer, A. Zevalkink, N. Crisosto, and G. J. Snyder, *Adv. Funct. Mater.* **20**, 4375 (2010).
- <sup>3</sup> A. Bentien, S. Johnsen, G. K. H. Madsen, B. B. Iversen, and F. Steglich, *E P L* **80**, 17008 (2007).
- <sup>4</sup> H. Takahashi, R. Okazaki, Y. Yasui, and I. Terasaki, *Phys. Rev. B* **84**, 205215 (2011), URL <http://link.aps.org/doi/10.1103/PhysRevB.84.205215>.
- <sup>5</sup> B. C. Sales, O. Delaire, M. A. McGuire, and A. F. May, *Phys. Rev. B* **83**, 125209 (2011), URL <http://link.aps.org/doi/10.1103/PhysRevB.83.125209>.
- <sup>6</sup> W. Liu, X. Tan, K. Yin, H. Liu, X. Tang, J. Shi, Q. Zhang, and C. Uher, *Phys. Rev. Lett.* **108**, 166601 (2012), URL <http://link.aps.org/doi/10.1103/PhysRevLett.108.166601>.
- <sup>7</sup> V. K. Zaitsev, M. I. Fedorov, E. A. Gurieva, I. S. Eremin, P. P. Konstantinov, A. Y. Samunin, and M. V. Vedernikov, *Phys. Rev. B* **74**, 045207 (2006), URL <http://link.aps.org/doi/10.1103/PhysRevB.74.045207>.
- <sup>8</sup> S. K. Bux, M. T. Yeung, E. S. Toberer, G. J. Snyder, R. B. Kaner, and J.-P. Fleurial, *J. Mater. Chem.* **21**, 12259 (2011).
- <sup>9</sup> T. Itohi and M. Yamada, *J. Electron. Mater.* **38**, 925 (2009).
- <sup>10</sup> Y. Sadia and Y. Gelbstein, *J. Electron. Mater.* **41**, 1504 (2012).
- <sup>11</sup> O. N. Il'nitskaya, V. A. Bruskov, P. Y. Zavali, and Y. B. Kuz'ma, *Inorganic Materials (USSR)* **27**, 1108 (1991).
- <sup>12</sup> *Acta Crystallogr. B* **28**, 3672 (1972).
- <sup>13</sup> C. Yang, F. Huang, L. Wu, and K. Xu, *J. Phys. D: Appl. Phys.* **44**, 295404 (2011).
- <sup>14</sup> E. J. Skoug, J. D. Cain, and D. T. Morelli, *Appl. Phys. Lett.* **98**, 261911 (2011).
- <sup>15</sup> E. J. Skoug, J. D. Cain, P. Majsztrik, M. Kirkham, E. Lara-Curzio, and D. T. Morelli, *Appl. Phys. Lett.* **3**, 602 (2011).
- <sup>16</sup> E. J. Skoug, J. D. Cain, D. T. Morelli, M. Kirkham, P. Majsztrik, and E. Lara-Curzio, *J. Appl. Phys.* **110**, 023501 (2011).
- <sup>17</sup> G. L. Vick and K. M. Whittle, *J. Electrochem. Soc.* **116**, 1142 (1969).
- <sup>18</sup> H. J. Goldsmid and J. W. Sharp, *J. Electron. Mater.* **28**, 869 (1999).
- <sup>19</sup> A. F. Ioffe, *Semiconductor Thermoelements and Thermoelectric Cooling* (Infosearch Ltd, London, 1957).
- <sup>20</sup> E. S. Toberer and G. J. Snyder, *Nature Materials* **7**, 105 (2008).